Jurnal Teknologi

Full Paper

DETAILED KINETICS OF TETRACYCLINE ADSORPTION IN AQUEOUS SOLUTION BY PALM SHELL-DERIVED ACTIVAED CARBON

Sasit Soisuwan[a], Ratanaporn Yuangsawad[b], Teruoki Tago[c], Duangkamol Na-Ranong[a]*

[a]Department of Chemical Engineering, School of Engineering, King Mongkut's Institute of Technology Ladkrabang, 10520, Bangkok, Thailand
[b]Division of Chemical Engineering, Faculty of Engineering, Rajamangala University of Technology Krungthep, 10120, Bangkok, Thailand
[c]Department of Chemical Science and Engineering, School of Materials and Chemical Technology, Institute of Science Tokyo, 152-8552, Tokyo, Japan

Article history
Received
3 June 2025
Received in revised form
13 November 2025
Accepted
18 December 2025
Published Online
29 August 2026

*Corresponding author
duangkamol.na@kmitl.ac.th

Graphical abstract

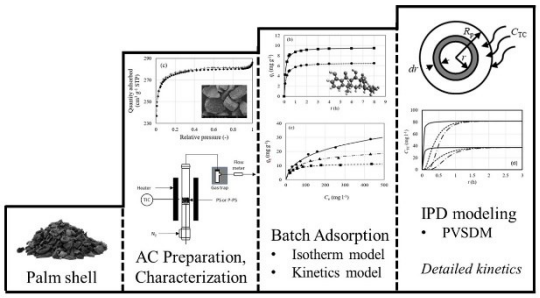

Abstract

The excessive excretion of antibiotics in wastewater poses significant environmental risks. Adsorption is expected as highly efficient, cost-effective, and sustainable methods for treating these contaminants. This study investigated the adsorption of tetracycline hydrochloride (TC) on palm shell derived activated carbon (PSAC) using the advanced pore volume and surface diffusion model (PVSDM). Scanning electron microscopy and N_2 adsorption isotherm revealed a highly microporous PSAC with a specific surface area of 852.85 $m^2 g^{-1}$, an average pore diameter of 2.068 nm and a micropore proportion of 0.72. In the developing PVSDM, conventional isotherms (e.g. Langmuir, Freundlich and Redlich-Peterson) and global kinetics models (e.g. pseudo-first order, pseudo-second order and Elovich) were comprehensively analyzed and the most suitable isotherm and global kinetics models were incorporated into the PVSDM. External film diffusion and intraparticle diffusion (IPD) investigation, according to Weber-Morris and Boyd, consistently confirmed strong IPD control. The PVSDM effectively reproduced time-dependent adsorption capacity in batch experiment and was verified by reasonable prediction of the dynamic change of adsorption capacity within the PSAC particle. The determined mass transfer parameters indicated that pore volume diffusion was the dominant mechanism, while surface diffusion was insignificant. This study demonstrates the effectiveness of PVSDM for quantifying mass transfer resistances in adsorption of TC on PSAC, providing valuable insights for the design and optimization of large-scale adsorption equipment for treatment of antibiotics in wastewater.

Keywords: Activated carbon, adsorption, pore volume and surface diffusion model, tetracycline, wastewater treatment

1.0 INTRODUCTION

The widespread use of antibiotics in medicine and food production has raised significant environmental concerns due to excessive excretion [1], which risk promoting antibiotic-resistant bacteria and affecting food and water supplies [2]. Recently, tetracycline antibiotics are frequently detected in influents of wastewater treatment facilities. For example, studies have reported the concentration as high as 61 mg l^{-1} in over 95% of surveyed facilities in northern China [3]. To address this challenge, among several methods that have been developed, adsorption is a promising technique for removing tetracyclines from wastewater [4-6].

In efforts to develop highly-efficient adsorbents for various applications, activated carbon (AC), particularly synthesized from renewable resources, has significantly attracted attention due to its high porosity and tunable surface properties [7, 8]. To evaluate the kinetics of adsorption, most previous research has primarily relied on batch adsorption experiments and employed global kinetics models such as pseudo-first order (PFO), pseudo-second order (PSO) and Elovich (EV) models. However, in the systems involving large-molecule adsorbates and high-porosity adsorbents with a significant proportion of micropores, as in the adsorption of tetracyclines on AC, the adsorption kinetics can be significantly influenced by a combination of external film diffusion (EFD), intraparticle diffusion (IPD) and surface interactions. Consequently, the global kinetics models may not accurately reflect the actual behavior of this adsorption system in practical applications, such as in packed-bed adsorbers.

For better understanding the behavior of adsorption system with strong hinder effects from mass transfer, simple diffusional kinetics models, including the Weber-Morris (WM) plot and Boyd (BD) analysis, have often used to characterize the effects of external and internal mass transfer, respectively, and identify the rate limiting step. Previous studies commonly reported IPD as the controlling mechanism in adsorption of tetracyclines on AC [4-6]. Since internal mass transfer resistance impedes the diffusion of adsorbate molecules within the porous structure of adsorbents, elevated internal resistance can reduce adsorption capacity, alter breakthrough curve profiles, and decrease column efficiency by limiting access to internal adsorption sites, accurate estimation of this resistance is essential for reliable scale-up from laboratory to industrial applications, optimization of operational parameters, and improved prediction of column performance. However, the estimation of internal adsorption resistance has been rarely reported in previous studies as many models simplify these processes for classification rather than detailed measurement of internal mass transfer resistance. To overcome the above-mentioned limitations, advanced modeling approaches, such as a pore volume and surface diffusion model (PVSDM), allow for the quantification of internal mass transfer resistance, should be inevitably considered.

This study employs the PVSDM, which incorporates internal mass transfer effects using a finite element approach to simulate pore structure in adsorbent particles and a numerical method to calculate kinetics parameters of the individual steps in adsorption of tetracycline hydrochloride (TC) onto AC prepared from palm shell. To achieve this, isothermal batch adsorption data, encompassing adsorption isotherm and adsorption kinetics, incorporate with the physical properties of adsorbent will be utilized in the development of PVSDM.

2.0 METHODOLOGY

2.1 Activated Carbon From Palm Shell (PSAC)

Palm shell-derived activated carbon (PSAC) was prepared as follows: palm shell (PS) was washed, dried, ground and sieved to particle size between 0.2 and 2 mm. It was then pyrolyzed under nitrogen flow at 773 K for 90 min. The pyrolyzed PS, with particle sizes between 0.2 and 0.3 mm, was impregnated with KOH aqueous solution (10 M) at the ratio of 10 ml g^{-1} and shaken at 190 rpm, 338 K for 2 h. The solid was then dried at 383 K for 1 h and thermally treated under N_2 flow at 1023 K for 1 h. After the thermal treatment, the solid was neutralized by distilled water, dried at 383 K for 6 h and stored in a desiccator.

Porous properties measured from nitrogen adsorption isotherm at 77 K (TriStar II Plus 3.02, Micromeritics); specific surface area (S_{BET}), external surface area (S), micropore volume (V_{micro}) and total pore volume (V_t) were calculated based on Brunauer-Emmett-Teller multi-point, Dubinin-Radushkevich method, t-plot and single point adsorption, respectively. An average pore diameter (d_{avg}) was calculated from $4V_t/S_{BET}$. Surface morphology and texture were observed by a scanning electron microscope (FEI Quanta 250 FEG Thermo Fisher Scientific, USA). Elements in PSAC were also analysed with energy dispersive spectroscopy (EDS) technique.

2.2 Adsorption Experiment

Tetracycline hydrochloride (AR grade, > 99%; Vesco Pharmaceutical Co., Ltd.), representing the tetracycline group of antibiotics, was selected to prepare a model wastewater and will be referred to as TC throughout this study.

The mixture of PSAC and TC aqueous solution (2 g l^{-1}) was shaken in an orbital shaker (KS 4000 ic, IKA). Initial concentration and temperature were varied from 30 to 490 mg l^{-1} and from 300 to 318 K, respectively. For kinetics investigations, two initial concentrations (50 and 100 mg l^{-1}) were selected, as these correspond to the industrially relevant range of TC levels [3]. Adsorption capacity (q) was calculated from $V(C_0–C)/m$. The concentration of TC solution was measured at 355 nm using Evolution 201 UV-Visible

spectrophotometer (Thermo Fischer Scientific). Calibration curve, constructed in the range of 1 – 30 mg l^{-1}, showed excellent linearity ($R^2 > 0.999$). The data were averaged from three replications and the errors of adsorption capacities were less than 2%.

2.3 Mathematical models and calculation methodology

Table 1 summarizes the mathematical models used to investigate isotherm (Langmuir (L), Freundlich (F), Redlich-Peterson (RP)), global kinetics (PFO, PSO, EV), diffusional kinetics (WM, BD) and mass transfer parameters (PVSDM).

For isotherm and global kinetics, model discrimination and parameter fitting were performed based on nonlinear regression analysis (NRA) where the initial guesses were estimated from linear regression analysis (LRA). To investigate the influence of external film diffusion (EFD) and intraparticle diffusion (IPD), and clarify the rate limiting step of the adsorption process, kinetics data was analyzed according to the WM and BD models, with the assumption of instantaneous adsorption onto active sites (AAS).

To estimate the mass transfer parameters, PVSDM, coupled with the selected isotherm (RP) and global kinetics (PSO) models were developed. The calculation methodology was applied in the same manner as described in previous work [9]. The external adsorption rate constant (k_{ext}, = 0.0402 and 0.0442 m h^{-1} at C_0 = 50 and 100 mg l^{-1}, respectively) and the molecular diffusivity of TC in aqueous solution (D_{AB}, 4.20×10^{-6} cm^2 s^{-1}) were estimated from initial rate according to PSO model and the method proposed by Wilke and Chang [10], respectively. As general assumption for AC [11, 12], tortuosity factor (τ) of 3.5 was used. The particle porosity (ε) was estimated from $\tau = (2-\varepsilon)^2/\varepsilon$. The initial guess of effective pore volume diffusion coefficient (D_{ep}) was determined from $D_{AB}\varepsilon/\tau$ [9]. The optimum D_{ep} was calculated using the Matlab® function lsqnonlin with the Trust-Region-Reflective algorithm, minimizing the sum of squared errors between experimental and model-derived adsorption capacities. Non-linear equations were solved using the Matlab® function fsolve with the Levenberg-Marquardt algorithm, while ordinary differential equations were addressed using ode15s, based on numerical differentiation formulas. Partial differential equations were discretized using finite difference approximations, employing second-order central difference approximations for the first and second derivatives, and second-order forward difference approximations to handle boundary conditions.

To validate the obtained models and parameters, the statistical parameters (R^2: coefficient of determination, *ARE*: average relative error, S_{RE}: standard deviation of relative error and *MPSD*: Marquardt's percent standard deviation) as well as the characteristic resemblance between the experimental data and the calculated result were considered. The calculation of statistical parameters is presented in previous study [13].

Table 1 Mathematical expressions and parameters of kinetic and isotherm models

Model	Nonlinear Form	Linear Form
	1. Adsorption Isotherm	
L	$q_e=\frac{q_L k_L C_e}{1+k_L C_e}$	$\frac{C_e}{q_e}=\frac{1}{q_L k_L}+\frac{C_e}{q_L}$
F	$q_e=k_F C_e^{1/n_F}$	$\ln(q_e)=\ln(k_F)+\frac{1}{n_F}\ln(C_e)$
RP	$q_e=\frac{k_{RP} C_e}{1+a_{RP} C_e^{b_{RP}}}$	–
	2. Global Kinetics	
PFO	$q_t=q_e(1-e^{-k_1 t})$	$\ln\left(\frac{q_e}{q_e-q_t}\right)=k_1 t$
PSO	$q_t=\frac{k_2 q_t^2 t}{1+k_2 q_e t}$	$\frac{t}{q_t}=\frac{1}{k_2 q_e^2}+\frac{t}{q_e}$
EV	$q_t=\left(\frac{1}{\beta}\right)\ln(1+\alpha\beta t)$	$q_t=\left(\frac{1}{\beta}\right)\ln(\alpha\beta)+\left(\frac{1}{\beta}\right)\ln(t)$ Assumption: $\alpha\beta t >> 1$
	3. Diffusional Kinetics	
WM	–	$q_{t,\,zi}=k_{zi}\sqrt{t}+C_{zi}$
BD	–	Bt=-0.498-ln(1-F) where $F = q_t/q_e$
PVSDM	$V\frac{dC_A}{dt}=-mSk_{ext}(C_A-C_{Ar\|r=R})$ $t = 0,\ C_A = C_{A0}$ $\varepsilon\frac{dC_{Ar}}{dt}+\rho\frac{dq}{dt}=\frac{1}{r^2}\frac{d}{dr}\left(r^2\left(D_{ep}\frac{dC_{Ar}}{dr}+\rho D_s\frac{dq}{dr}\right)\right)$ $t = 0,\ 0 \le r \le R_p,\ C_{Ar} = 0$ $r = 0,\ \frac{dC_{Ar}}{dr}\Big\|_{r=0}=0$ $r = R,\ D_{ep}\frac{dC_{Ar}}{dr}\Big\|_{r=R}+\rho D_s\frac{dq}{dr}\Big\|_{r=R}=k_{ext}(C_A-C_{Ar\|r=R})$	

3.0 RESULTS AND DISCUSSION

3.1 Characteristic of PSAC

SEM images in Figure 1 show that PSAC has spongy structure with numerous internal pores and cavities of various shapes and sizes, without any cracks and debris, indicating successful porous structure development by KOH activation. EDS analysis revealed a uniform dispersion of C (86.27 wt %), O (11.83 wt %) and traces of alkaline metals including K (0.42 wt %), Mg (0.32 wt %), and Ca (0.73 wt %) on the

surface of PSAC. Figure 1 (c) shows that N_2 adsorption isotherm of PSAC has characteristic of type I isotherm according to IUPAC (International Union of Pure and Applied Chemistry) classification, indicating that micropores predominantly existed in PSAC structure. S_{BET}, V_t, V_{micro} and d_{avg} were 852.85 m^2 g^{-1}, 0.4409 cm^3 g^{-1}, 0.3180 cm^3 g^{-1} (micropore > 72%) and 2.068 nm, respectively. Micropore fraction and d_{avg} indicate that pore size distribution is positive skew (d_{mode} < d_{median} < d_{avg}) due to more than 72% of population is micropore.

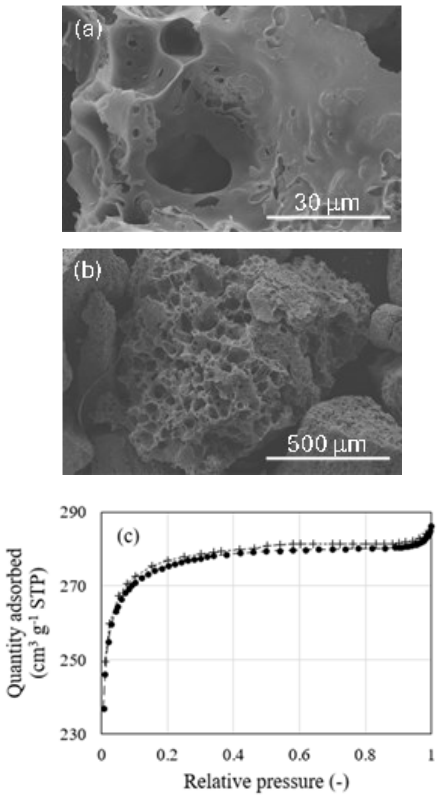

Figure 1 Porous properties of PSAC: (a, b) SEM images of PSAC at different magnifications; (c) N_2 adsorption and desorption isotherms

3.2 Adsorption isotherm

Isotherm experimental data (Figure 2) clearly shows that the amount of TC absorbed on PSAC at equilibrium (q_e) increased with the equilibrium concentration of TC (C_e) and the saturation (q_{sat}) was observed only at 300 K, around 10.52 mg g^{-1}. In addition, q_e increased with the adsorption temperature and the increase of q_e was more significant at the higher C_e.

Regression analysis (Table 2 and line plots in Figure 2) indicates that the isotherm data are best described by the L model at lower temperatures ($T \leq 309$ K) and the F model at higher temperatures. In contrast, the RP model could accurately represent the entire range of the experimental data, with R^2 of 0.9898 – 0.9933. At 300 K, the b_{RP} value was approximately 1, suggesting that the RP model reduces to L model. However, at higher temperatures (309 and 318 K), the b_{RP} value decreases with increase in temperature, indicating stronger characteristic of the F model.

3.3 Global Kinetics

Figure 3 compares the predicted adsorption capacity profiles, calculated using the nonlinear forms of PFO, PSO, and EV models with the model parameters estimated from NLA (Table 3), to the experimental data. The resemblance of the predicted curve with the experimental result, the statistical parameters (R^2, *ARE*, S_{RE} and *MPSD*) and Δq_e indicate that PSO provides the best fit, followed by PFO and then EV. The good fits of adsorption kinetic data with PSO model have been widely reported for adsorption of other large molecular dyes and petrochemicals from aqueous solution using cellulose-based adsorbents [14, 15]. This consistency was considered because of strong retardation effect from IPD in a network of fine pores and significant depletion of bulk concentration. Therefore, the kinetics data were further analyzed based on diffusional models to elaborate the influence of IPD.

3.4 Diffusional Mechanisms

WM plots in Figure 4 (a) obviously display multi-linearity in both cases and all the straight lines have positive intercept values (Table 4). This indicates that both IPD and EFD influenced the overall adsorption process [16]. In zone 1, the intercept values were slightly positive ($C_{z1} \approx 0$), indicating that the overall process was mainly controlled by IPD [17]. As the adsorption progresses, the bulk concentration of TC solution and the number of vacant sites decrease. Consequently, the EFD effect becomes more significant in zone 2. The adsorption finally reaches the equilibrium in zone 3. According to the BD model, the plot between [-ln(1-*F*)] and *t* should be a straight line passing through the origin if the overall adsorption process is controlled by EFD. However, in Figure 4 (b), the straight lines do not pass through the origin, indicating that the rate of adsorption is either controlled by IPD or combination of strong IPD and weak EFD. Both WM and BD models consistently suggested that the overall rates were dominantly affected by IPD with relatively weak effect of EFD.

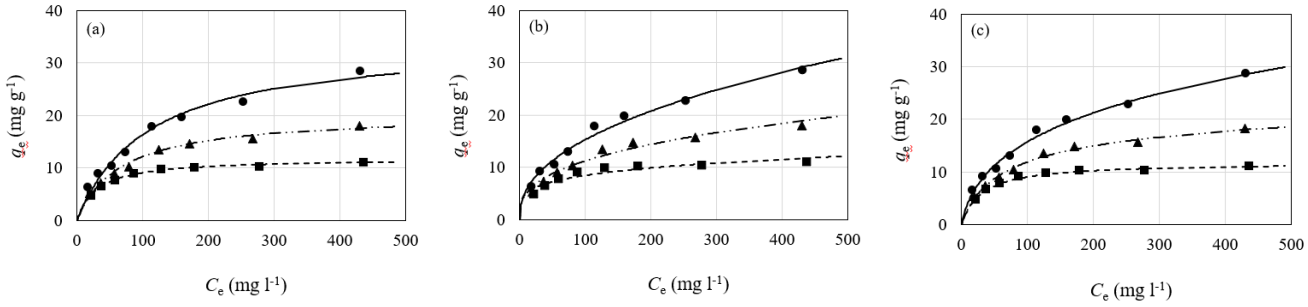

Figure 2 Isotherm fitting for TC adsorption on PSAC according to (a) L, (b) F, and (c) RP models at various temperatures; T = 300 K (o, - - -), T = 309 K (Δ, – · · –), and T = 318 K (×, ——)

Table 2 Model parameters of isotherm models and statistical parameters

Model	Parameter		LRA			NRA		
	Symbol	Unit	300 K	309 K	318 K	300 K	309 K	318 K
L	q_L	mg g^{-1}	11.74	20.58	34.25	11.81	20.36	34.30
	k_L	l mg^{-1}	0.0337	0.0146	0.0096	0.0329	0.0148	0.0091
	R^2	-	0.9905	0.9852	0.9744	0.9908	0.9856	0.9763
	ARE	-	2.1138	4.6859	8.7268	1.8565	4.7478	8.6743
	SRE	-	2.2673	5.0549	9.5301	2.0013	5.0556	9.1526
	MPSD	%	2.6157	6.9059	11.8152	2.4264	6.8045	12.4926
F	k_F	mg g^{-1} (l mg^{-1})$^{1/n}$	2.4342	1.7517	1.7225	2.9835	2.1735	1.9900
	n_F	-	3.7411	2.4981	2.1209	4.4267	2.8031	2.2598
	R^2	-	0.8513	0.9501	0.9818	0.8790	0.9635	0.9858
	ARE	-	8.4330	5.6325	4.5251	8.3163	6.4949	5.1493
	SRE	-	2.3988	5.1262	9.4096	2.1382	5.1863	9.3641
	MPSD	%	11.0242	7.5420	6.0613	12.6768	9.5197	7.2915
RP	k_{RP}	l g^{-1}				0.3425	0.3961	0.7065
	a_{RP}	l mg^{-1}				0.0223	0.0397	0.1403
	b_{RP}	-				1.0448	0.8839	0.6979
	R^2	-				0.9933	0.9898	0.9909
	ARE	-				1.3520	3.6071	4.4396
	SRE	-				1.9934	5.0865	9.2926
	MPSD	%				2.1303	5.2195	6.6370

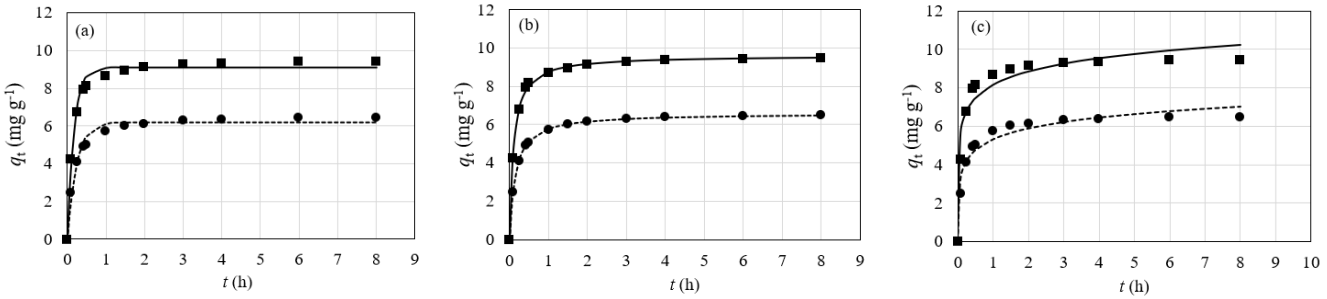

Figure 3 Comparison of kinetics models for TC adsorption on PSAC at C_0 = 50 (●) and 100 (■) mg l^{-1}: (a) PFO, (b) PSO, and (c) EV.

Table 3 Model parameters and statistical parameters of adsorption kinetics models

Model	Parameter		LRA		NRA	
	Symbol	Unit	C_0 (mg l^{-1})			
			50	100	50	100
PFO	q_e	mg g^{-1}	6.49	9.47	6.19	9.10
	k_1	h	1.0348	1.1324	4.2615	5.9182
	R^2	-	0.6578	0.5764	0.9745	0.9816
	ARE	-	26.9691	27.2084	5.7041	4.4899
	SRE	-	27.0977	30.5530	5.9527	4.6982
	MPSD	%	42.8294	43.6420	9.7420	6.7808
	Δq_e	%	-	-	-4.62	-3.91
PSO	q_e	mg g^{-1}	6.58	9.55	6.59	9.60
	k_2	g h^{-1} mg^{-1}	1.2208	1.2747	1.0665	1.0616
	R^2	-	0.9925	0.9941	0.9992	0.9992
	ARE	-	2.1838	2.1098	0.7551	1.0029
	SRE	-	2.3891	2.0982	0.8008	1.0662
	MPSD	%	3.5413	4.7985	1.2383	1.6137
	Δq_e	%	1.44	0.86	1.48	1.38
EV	α	mg g^{-1} h^{-1}	507.74	3309.66	524.54	3381.67
	β	g mg^{-1}	1.2077	0.9961	1.2146	0.9984
	R^2	-	0.9606	0.9480	0.9634	0.9518
	ARE	-	7.2267	7.3234	7.2405	7.2999
	SRE	-	7.5930	7.7100	7.6264	7.6934
	MPSD	%	11.8592	12.3525	12.0593	12.4156

3.5 Validation of PVSDM and Determination of Mass Transfer Parameters

Figure 4 (c) shows time-dependence of bulk concentration of TC. The best fit of PVSDM with the experimental result was obtained with $R^2 > 0.9946$ and the optimum D_s and D_{ep} were listed in Table 4. The changes of C_{TC} and q_{TC} with adsorption time at various radial positions were reasonably predicted as illustrated in Figure 4 (d) and (e), respectively. It can be seen that C_{TC} at the external surface ($r = R$) rapidly increased and reached the equilibrium within 35 min for both cases ($C_{TC,0}$ = 50 and 100 mg l^{-1}) while C_{TC} inside the particle at the smaller R-position took the longer time to reach the local equilibrium (q_t/q_e = 0.99); at $C_{TC,0}$ = 50 mg l^{-1}, $t_{eq,\,r=0.5R}$ = 120 and $t_{eq,\,r=0}$ = 125 min whereas at $C_{TC,0}$ = 100 mg l^{-1}, $t_{eq,\,r=0.5R}$ = 85 and $t_{eq,\,r=0}$ = 90 min. Additionally, the lower initial concentration requires longer time to reach the local equilibrium.

The value of D_s is notably smaller than D_{ep} ($D_{ep}/D_s \approx 0.87 - 1.72\times10^5$), implying that the surface diffusion is significantly slower than the parallel pore diffusion, and thus can be neglected in the overall adsorption process. The estimated D_{ep} insignificantly varied with the initial concentration and significantly smaller than the initial guess value ($D_{ep,\,initial\ guess} = 185 D_{ep,\,estimate}$) [18-19]. This result is generally expected for systems with small-pore adsorbents and large adsorbates [9, 20]. Therefore, the result indicates that the adsorption of large TC molecules (0.95 – 1.27 nm [4]) in PSAC with small pore diameter (d_{mode} < 2 nm) was significantly hindered by IPD ($k_{ext}R/D_{ep} \approx 4.59 - 4.77\times10^3$).

Unlike the lump kinetics parameter in the PSO model with limited physical meaning, and indication of the dominant mass transfer steps according to the WM and BD models, the PVSDM parameters (D_{ep}, D_s, and k_{ext}) confirm that internal mass transfer resistance is the root cause of the low q_e, thereby providing clear, quantitative guidance for the structural modification of PSAC in future work (e.g., increasing mesopore fraction).

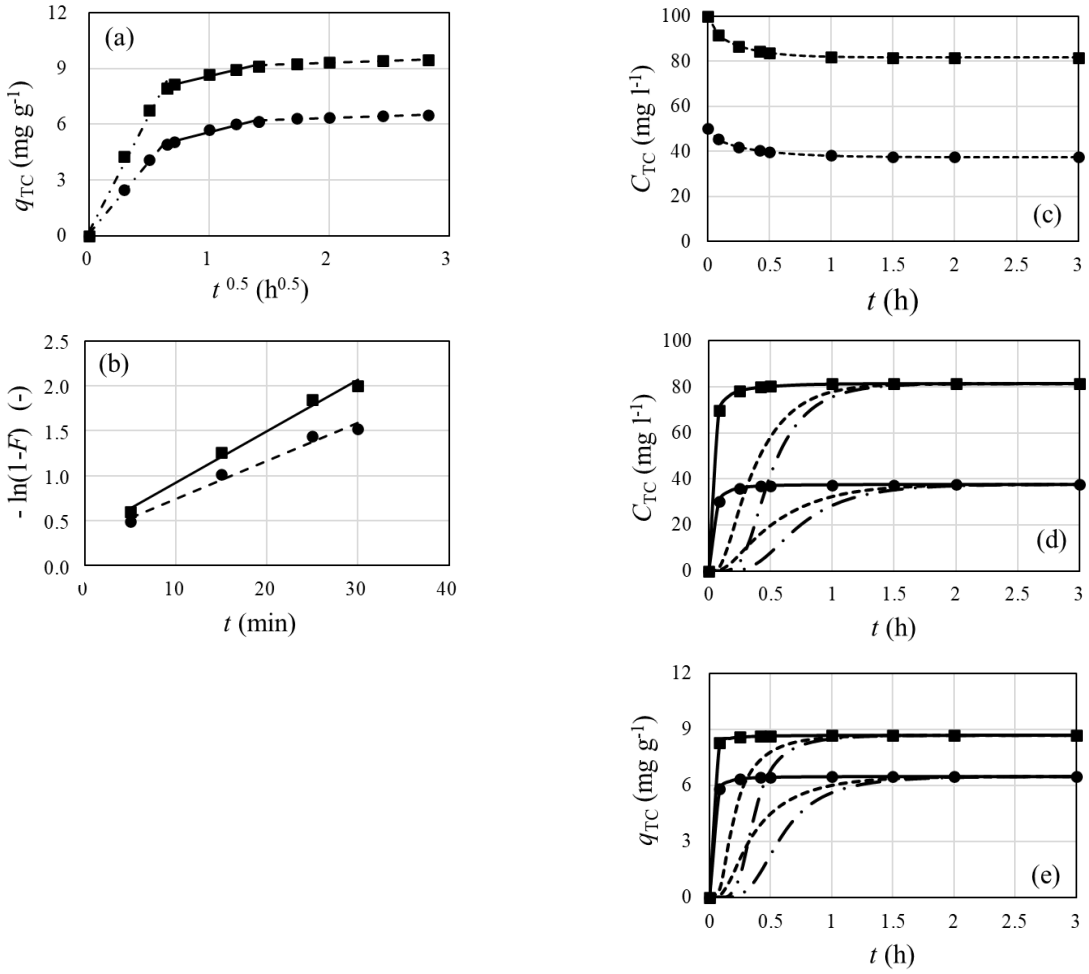

Figure 4 Kinetics analysis for TC adsorption on PSAC at C_0 = 50 (●) and 100 (■) mg l^{-1} according to (a) WM, (b) BD, and PVSDM (c) Bulk concentration decay curves, (d) Intraparticle concentration profile, and (e) Intraparticle adsorption capacity profiles at different radial position: at $r = 0$ (– · –), $0.5R$ (- - -), and R (——); symbols represent experimental data; lines represent calculated results.

Table 4 Model parameters and statistical parameters of diffusional kinetics models

Model		Parameter	Unit	C_0 (mg l^{-1})	
				50	100
WM	**zone 1**	k_{z1}	mg g^{-1} $h^{-0.5}$	7.7363	12.4720
		C_{z1}	mg g^{-1}	0.1130	0.2733
		R^2	-	0.9942	0.9883
	zone 2	k_{z2}	mg g^{-1} $h^{-0.5}$	1.6573	1.5268
		C_{z2}	mg g^{-1}	3.9234	7.0591
		R^2	-	0.9633	0.9711
	zone 3	$k_{z,3}$	mg g^{-1} $h^{-0.5}$	0.2271	0.2240
		C_{z3}	mg g^{-1}	5.8835	8.8663
		R^2	-	0.9063	0.9170
BD		B	min^{-1}	0.0476	0.0570
		c	-	0.2649	0.3565
		R^2	-	0.9968	0.9898
PVSDM		D_s	cm^2 s^{-1}	4.21×10^{-14}	2.24×10^{-14}
		D_{ep}	cm^2 s^{-1}	3.65×10^{-9}	3.86×10^{-9}
		k_{ext}	m h^{-1}	0.0402	0.0442
		S	m^2 g^{-1}	26.31	26.31
		R^2	-	0.9946	0.9960
		ARE	-	0.9467	1.4340

4.0 CONCLUSION

This study successfully applied the sophisticated pore volume and surface diffusion model (PVSDM) to determine mass transfer parameters of the individual steps in the adsorption of TC using palm shell derived activated carbon (PSAC), a material characterized by a large specific surface area (S_{BET} = 852.85 m^2 g^{-1}) and high proportion of micropores (V_{micro}/V_t = 0.72 and d_{avg} = 2.068 nm). The PVSDM was developed based on comprehensive analysis of isothermal batch adsorption data; isotherm and global kinetics were most accurately described by Redlich-Peterson model (RP) and pseudo-second order model (PSO), respectively. Diffusional kinetics models, Weber-Morris (WM) and Boyd (BD) plots, consistently confirmed that this adsorption system was dominantly controlled by intraparticle diffusion (IPD) with weak effect of external film diffusion (EFD). The values of mass transfer parameters estimated by PVSDM approach uniformly indicated the dominance of IPD as the rate controlling step; $k_{ext}R/D_{ep} \approx 4.59 - 4.77\times10^3$ and $D_{ep}/D_s \approx 0.87 - 1.72\times10^5$. This advanced approach should be valuable for designing other adsorption systems, particularly those involving large adsorbate molecules and adsorbents with a high proportion of micropores. By providing a more accurate understanding of mass transfer processes, this approach can enhance the efficiency and operational reliability of the large-scale adsorbers.

Acknowledgement

This work was supported by the School of Engineering, King Mongkut's Institute of Technology Ladkrabang [2564-02-01-014] and the King Mongkut's Institute of Technology Ladkrabang [KREF016320]. The authors also thank Vesco Pharmaceutical Co., Ltd. for providing the tetracycline hydrochloride.

Conflicts of Interest

The authors declare that there is no conflict of interest regarding the publication of this paper.

References

[1] Chopra, I., and M. Roberts. 2001. Tetracycline Antibiotics: Mode of Action, Applications, Molecular Biology, and Epidemiology of Bacterial Resistance. *Microbiology and Molecular Biology Reviews*. 65: 232–260.

[2] Minarini, L. A. D. R., L. N. de Andrade, E. De Gregorio, F. Grosso, T. Naas, R. Zarrilli, and I. L. B. C. Camargo. 2020. Editorial: Antimicrobial Resistance as a Global Public Health Problem: How Can We Address It? *Frontiers in Public Health*. 8: 1–6.

[3] Hou, J., C. Wang, D. Mao, and Y. Luo. 2016. The Occurrence and Fate of Tetracyclines in Two Pharmaceutical Wastewater Treatment Plants of Northern China. *Environmental Science and Pollution Research*. 23: 1722–1731.

[4] Martins, A. C., O. Pezoti, A. L. Cazetta, K. C. Bedin, D. A. S. Yamazaki, G. F. G. Bandoch, T. Asefa, J. V. Visentainer, and V. C. Almeida. 2015. Removal of Tetracycline by NaOH-Activated Carbon Produced from Macadamia Nut Shells: Kinetic and Equilibrium Studies. *Chemical Engineering Journal*. 260: 291–299.

[5] Marzbali, M. H., M. Esmaieli, H. Abolghasemi, and M. H. Marzbali. 2016. Tetracycline Adsorption by H_3PO_4-Activated Carbon Produced from Apricot Nut Shells: A Batch Study. *Process Safety and Environmental Protection* 102: 700–709.

[6] Huang, H., J. Tang, K. Gao, R. He, H. Zhao, and D. Werner. 2017. Characterization of KOH Modified Biochars from Different Pyrolysis Temperatures and Enhanced Adsorption of Antibiotics. *RSC Advances*. 7: 14640–14648.

[7] Hidayu, A. R., N. F. Mohamad, S. Matali, and A. S. A. K. Sharifah. 2013. Characterization of Activated Carbon Prepared from Oil Palm Empty Fruit Bunch Using BET and FT-IR Techniques. *Procedia Engineering*. 68: 379–384.

[8] Hidayu, A. R., and N. Muda. 2016. Preparation and Characterization of Impregnated Activated Carbon from Palm Kernel Shell and Coconut Shell for CO_2 Capture. *Procedia Engineering*. 148: 106–113.

[9] Souza, P. R., G. L. Dotto, and N. P. G. Salau. 2017. Detailed Numerical Solution of Pore Volume and Surface Diffusion Model in Adsorption Systems. *Chemical Engineering Research and Design*. 122: 298–307.

[10] Wilke, C. R., and P. Chang. 1955. Correlation of Diffusion Coefficients in Dilute Solutions. *AIChE Journal*. 1: 264–270.

[11] Shi, S., A. Luo, J. Hao, S. Xie, and J. Feng. 2023. "Three-Dimensional Mass Transfer Modeling of Hydroquinone Adsorption on *Phragmites australis* Biochar. *Toxics*. 11: 1–13.

[12] Abdel Daiem, M. M., M. Sánchez-Polo, A. S. Rashed, N. Kamal, and N. Said. 2019. Adsorption Mechanism and Modelling of Hydrocarbon Contaminants onto Rice Straw Activated Carbons. *Polish Journal of Chemical Technology*. 21: 1–12.

[13] Benoit, B., Pierre Le Cloirec, and Dominique W. 2008. Revisiting the Determination of Langmuir Parameters—Application to Tetrahydrothiophene Adsorption onto Activated Carbon. *Langmuir*. 24: 6420–6424.

[14] Hubbe, M., S. Azizian, and S. Douven. 2019. Implications of Apparent Pseudo-Second-Order Adsorption Kinetics onto Cellulosic Materials: A Review. *BioResources*. 14: 7582–7626.

[15] Hubbe, M. A., J. Park, and S. Park. 2014. "Cellulosic Substrates for Removal of Pollutants from Aqueous Systems: A Review. Part 4. Dissolved Petrochemical Compounds." *BioResources* 9: 7782–7925.

[16] Tran, H. N., S. J. You, A. Hosseini-Bandegharaei, and H. P. Chao. 2017. Mistakes and Inconsistencies Regarding Adsorption of Contaminants from Aqueous Solutions: A Critical Review. *Water Research*. 120: 88–116.

[17] Wang, J., and X. Guo. 2022. Rethinking of the Intraparticle Diffusion Adsorption Kinetics Model: Interpretation, Solving Methods and Applications. *Chemosphere*. 309: 136732.

[18] Wang, G., Z. T. Chen, X. Y. Lan, W. Wang, C. M. Xu, and J. S. Gao. 2011. Restricted Diffusion of Residual Molecules in Catalyst Pores under Reactive Conditions. *Chemical Engineering Science*. 66: 1200–1211.

[19] Fogler, H. Scott. 2006. *Elements of Chemical Reaction Engineering*. 4th ed. Upper Saddle River, NJ: Prentice Hall, 814–816.

[20] Fröhlich, A. C., R. Ocampo-Pérez, V. Diaz-Blancas, N. P. G. Salau, and G. L. Dotto. 2018. Three-Dimensional Mass Transfer Modeling of Ibuprofen Adsorption on Activated Carbon Prepared by Sonication. *Chemical Engineering Journal*. 341: 65–74.